Geochemistry Geophysics Geosystems G3

Article
Volume 14, Number XX
XX Month 2013
doi:10.1002/ggge.20045
ISSN: 1525-2027

Published by AGU and the Geochemical Society

Seasonal moisture sources and the isotopic composition of precipitation, rivers, and carbonates across the Andes at 32.5–35.5°S

Gregory D. Hoke
Department of Earth Sciences, Syracuse University, Syracuse, NY, 13244, USA (gdhoke@syr.edu)

Julieta N. Aranibar
Instituto Argentino de Nivología, Glaciología y Ciencias Ambientales, CCT, Mendoza, Argentina

Instituto de Ciencias Básicas, Universidad Nacional de Cuyo, Mendoza, Argentina

Maximiliano Viale
Instituto Argentino de Nivología, Glaciología y Ciencias Ambientales, CCT, Mendoza, Argentina

Departamento de Geofísica, Facultad de Ciencias Físicas y Matemáticas, Universidad de Chile, Santiago, Chile

Diego C. Araneo
Instituto Argentino de Nivología, Glaciología y Ciencias Ambientales, CCT, Mendoza, Argentina

Carina Llano
Departamento de Antropología, Museo de Historia Natural de San Rafael, San Rafael, Mendoza, Argentina

[1] Constraining the influence of different moisture sources across the flanks of mountain ranges is important for understanding tectonic, geomorphic, and paleoclimate problems at geologic timescales, as well as evaluating climate change and water resources on human time scales. The stable isotope compositions of stream waters and precipitation are an ideal tool for this task. This study reports the results of a 2 year monthly precipitation sampling campaign on the eastern flank of the Andes in the Mendoza Province of Argentina, which began in September 2008. A total of 104 precipitation samples spanning some 2500 m of relief from nine sites were analyzed for δD and $\delta^{18}O$. In addition, 81 samples from Andean rivers collected on both sides of the range in 2002 and 2007 were analyzed. We employ a Rayleigh isotope fractionation modeling approach to explore spatial and temporal variations in precipitation and river water compositions. The results indicate that precipitation on the eastern slopes of the Andes at ~33°S, at elevations above 2 km, is largely derived from a westerly, Pacific-source component and a mixture of easterly and westerly sources below 2 km. Further south at ~35°S, river water compositions exhibit a strong winter influence. At 33°S, rivers have an isotopic minimum of ~ −18‰ across the core of the range, which has an average elevation of 4000 m, and are topographically offset from similar isotopic values of precipitation by +1000 m. Comparison of precipitation and river water data with temperature-corrected $\delta^{18}O$ estimates from pedogenic carbonates illustrates that carbonates capture the range of variability observed in modern precipitation and Rayleigh fractionation models.

Components: 10,600 words, 7 figures, 2 tables.

Keywords: stable isotopes; precipitation; rivers; pedogenic carbonate; Andes; South America.

Index Terms: 1041 Geochemistry: Stable isotope geochemistry (0454, 4870); 3354 Geochemistry: Precipitation (1854); 4914 Geochemistry: Continental climate records;

Received 3 July 2012; **Revised** 11 December 2012; **Accepted** 13 December 2012; **Published** XX Month 2013.

Hoke G. D., Aranibar J. N., Viale M., Araneo D. C. and Llano C. (2013), Seasonal moisture sources and the isotopic composition of precipitation, rivers, and carbonates across the Andes at 32.5–35.5°S, *Geochem. Geophys. Geosyst.*, *14*, doi:10.1002/ggge.20045.

1. Introduction

[2] Isotopic data on mountain precipitation are sparse yet essential to refining isotope tracking modules in climate models [e.g., *Jeffery et al.*, 2012; *Sturm et al.*, 2007; *Vuille et al.*, 2003], statistical models of isotopes in precipitation [e.g., *Bowen and Wilkinson*, 2002], and the interpretation of stable isotope archives thought to primarily reflect paleo-precipitation [e.g., *Cerling and Quade*, 1993; *Kleinert and Strecker*, 2001; *Masiokas et al.*, 2006; *Polissar et al.*, 2009]. Isotopic characterization of mountain precipitation also allows for the tracking of moisture sources to examine interannual variability in regional-scale climate and to differentiate geographic and hydrogeologic water sources to rivers [*Wassenaar et al.*, 2011]. In the context of recent climate change and the consequent recession of glaciers [*Masiokas et al.*, 2006], characterization of the relative importance of different moisture sources on mountain river basins is critical to understand changes in river behavior and to potentially develop mitigation plans for future climate and glacier mass changes.

[3] With monthly data from more than 900 stations worldwide, the Global Network of Isotopes in Precipitation (GNIP; *IAEA* [2006]) provides a globally synoptic view of isotopes; however, less than 10% of GNIP stations are at elevations above 2 km, and only a small number of these stations reflect elevation transects up the sides of mountain ranges [*Gonfiantini et al.*, 2001]. Of the high elevation stations (>2 km), nearly 65% are located on the South American continent, and the majority of these are within 10° of tropical latitudes spanning the Puna/Altiplano Plateau, including the only high elevation station in Argentina (Figure 1a). The collection of additional stable isotope data from the high topography of South America outside of topical latitudes enhances our ability to understand how the water isotopes change as the range narrows and transitions into the midlatitude westerly winds.

[4] The development of paleoaltimetry in Asia [e.g., *Garzione et al.*, 2000; *Rowley and Currie*, 2006], the western U.S. [*Mulch et al.*, 2006], and South America [*Garzione et al.*, 2008] over the last 15 years has called into question the fidelity of isotopic archives as faithful recorders of paleo-precipitation [e.g., *Ehlers and Poulsen*, 2009; *Jeffery et al.*, 2012; *Lamb*, 2011]. However, even as stable isotope paleoaltimetry expands through increased application to pedogenic carbonate [*Rowley and Garzione*, 2007], plant wax biomarkers [*Sauer et al.*, 2001], and the potential use of clumped isotopes [*Ghosh et al.*, 2006; *Peters et al.*, 2013], questions regarding the ability of these and similar geologic archives to provide meaningful representations of surface conditions will persist unless the modern system is examined holistically.

[5] We present isotopic data from 2 years of quasi-monthly precipitation sampling on the subtropical eastern flanks of the southern Central Andes (32.5–35.5°S), an area with some of the highest elevations outside the Andean Plateau collected between September 2008 and October 2010. The data fill an important gap between prior work in high midlatitudes of Patagonia [*Stern and Blisniuk*, 2002] and the tropics of Bolivia [*Gonfiantini et al.*, 2001]. We also augment existing data on Andean rivers [*Hoke et al.*, 2009; *Vogel et al.*, 1975] with 81 new analyses of river water data. Our isotopic data are compared to Rayleigh isotope fractionation fraction models of

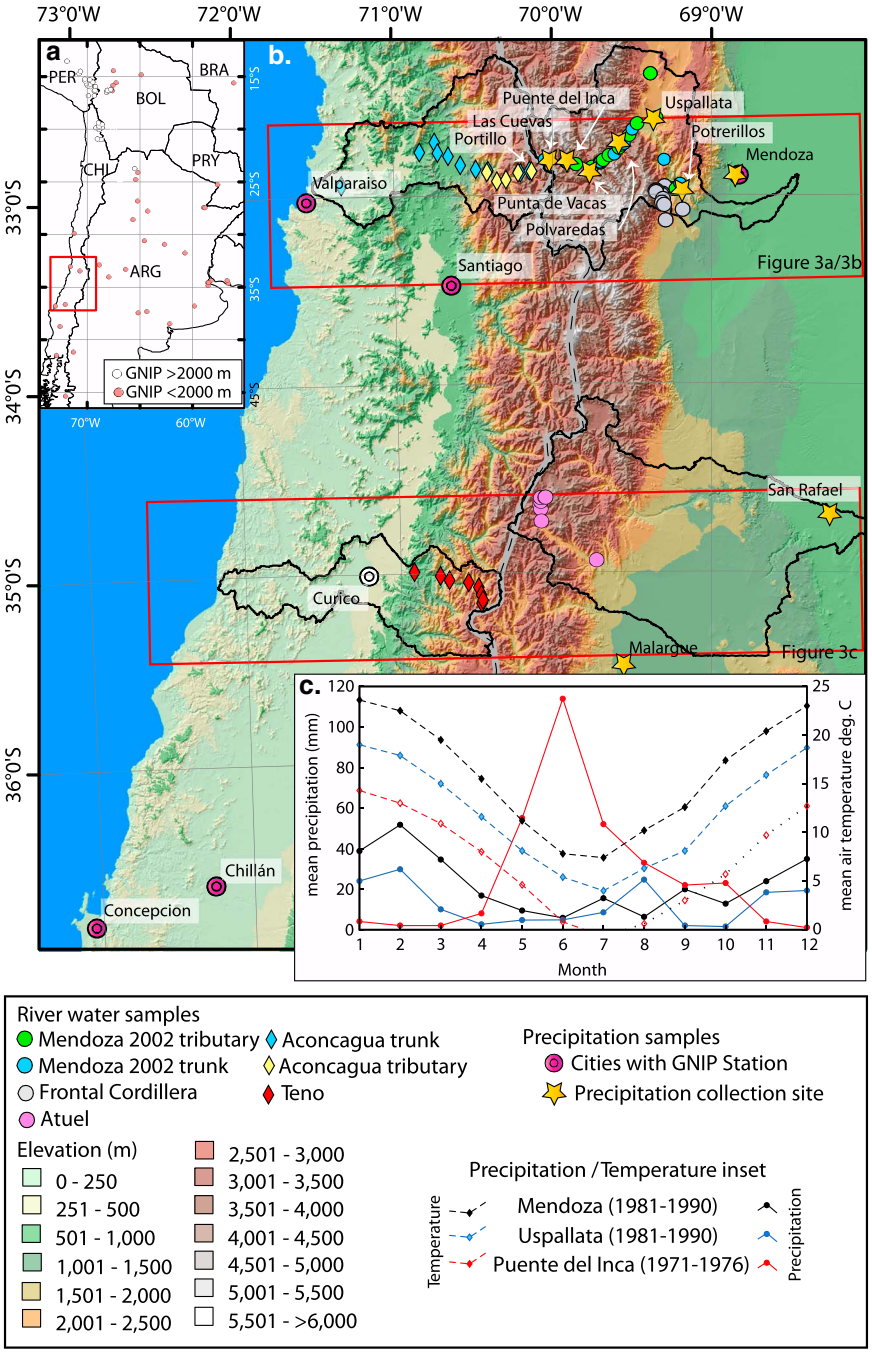

Figure 1. (a) Map of South America showing the location of GNIP monthly precipitation sampling sites above 2 km (white circles) and below 2 km (red dots). The area shown in Figure 1b is outlined by the red box. (b) Location of river water sampling sites (colored circles) and precipitation sampling sites (purple concentric circles). Light blue concentric circles mark the locations of GNIP stations. Watersheds are delineated by the black outlines enclosing river water sample sites. The white-dashed black line is the Andean drainage divide and political boundary between Argentina and Chile. (c) Average precipitation and temperature data for Punta de Vacas, Uspallata, and Mendoza, Argentina from the Argentine Servicio Meteorological Nacional stations. Station data reveal the west to east change in precipitation, with a winter dominance in the west at Punta de Vacas, mixed signal at Uspallata, and summer dominance at Mendoza.

seasonal air mass water vapor originating in the lowlands of Argentina and Chile. Finally, we compare precipitation and river water isotope compositions to soil water values calculated from pedogenic carbonate $\delta^{18}O$ values using temperatures derived from clumped isotope analysis [*Peters et al.*, 2013].

2. Geography and Climate

2.1. Geography

[6] Spanning nearly 70° of latitude, the Andes are a major barrier to the circulation of the global winds in the Southern Hemisphere. Here, we focus on the southernmost central Andes between 32.5°S and 35.5°S, an area that lies on the northern flank of the westerlies, where precipitation is controlled by winter storm tracks and by weak, midlevel troughs, which trigger convective storms in summer (Figure 2). The range at these latitudes has the highest mean topography outside of the Central Andean Plateau, with average elevations of 4 km, average maximum topography of 5 km, and several peaks with elevations in excess of 6 km; thus, it forms a significant barrier to moisture sources from the Atlantic and Pacific oceans (Figure 2) [*Viale and Norte*, 2009; *Viale and Nuñez*, 2011] The physiographic provinces of the range from west to east are the Coastal Cordillera, Central Valley, Chilean Precordillera, Principal Cordillera, Frontal Cordillera, and the Precordillera finally giving way to the Pampas (Plains) (Figure 3). Total range height and width also decreases towards the south (Figure 1). Both the eastern and western flanks of the range are steep topographic fronts with local relief in excess of 1.5 km everywhere and locally exceeding 2.5 km (Figure 1).

2.2. Climate

[7] The climate of the subtropical central Andes and its surroundings has been described by pioneering studies covering Argentina, Chile, and all of South America [*Hoffmann*, 1975; *Miller*, 1976; *Prohaska*, 1976]. The transition between easterly and westerly winds has large annual and interannual variation with an average position of ~32°S. The average position appears to have been stable since the Last Glacial Maximum [*Haselton et al.*, 2002]. Climatic studies in our area emphasize the strong effect of the Andes in altering climate across adjacent lowlands on both sides of the range [*Ereño and Hoffmann*, 1978; *Viale and Nuñez*, 2011]. Ascent of air masses over mountain ranges strongly modifies precipitation amount [*Roe*, 2005] and isotopic composition [*Dansgaard*, 1964; *Sturm et al.*, 2007]. South of 30°S, Pacific-sourced moisture is mainly discharged on the western flank of the Andes during austral winter. Low $\delta^{18}O$ and δD spillover moisture from the west crosses the range and accounts for nearly all precipitation at elevations >2400 m and is nearly absent at the foot of the mountains (Figures 1c and 2b). Such an effect has been documented previously in river and rainfall in the Patagonian Andes [e.g., *Smith and Evans*, 2007; *Stern and Blisniuk*, 2002]. Likewise, Atlantic-source moisture, largely from the low-level Andean jet, condenses and precipitates on the eastern flank and foothills of the southern central Andes as summer convective storms. Only under certain atmospheric conditions, such as low-level high-pressure moving along eastward over central Argentina or a midlevel trough just west of the Andes, does Atlantic-derived moisture penetrate into the core and western flanks of the range (Figure 2c).

[8] As a consequence of the southward migration of storm tracks, summer precipitation on the lowlands

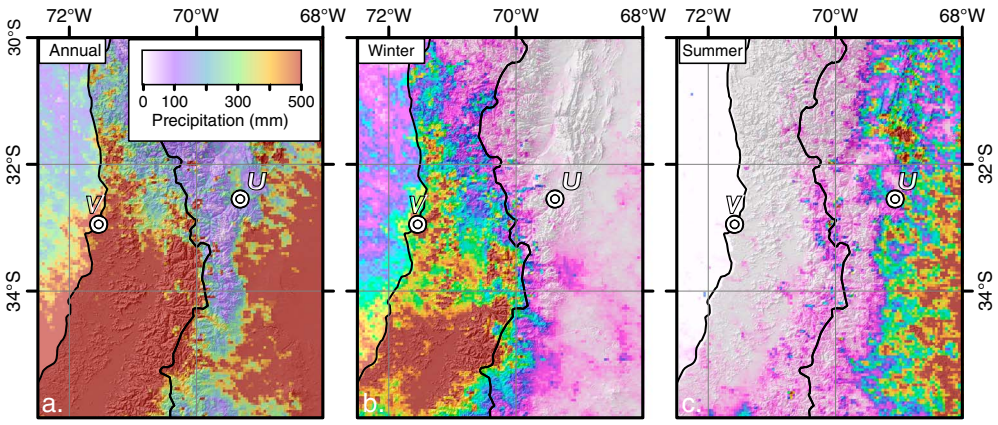

Figure 2. Synoptic view of (a) annual, (b) winter, and (c) summer precipitation patterns derived from using Tropical Rainfall Measuring Mission data [*Bookhagen and Strecker*, 2008] over the 12 year period from 1998 to 2009. Valparaiso (V) and Uspallata (U) are labeled with a bulls-eye symbol on all maps. Winter precipitation dominates the western flank of the Andes, with spillover visible in the TRMM data below 32°S and especially near 35°S. Summer precipitation is largely confined to the eastern flanks of the range.

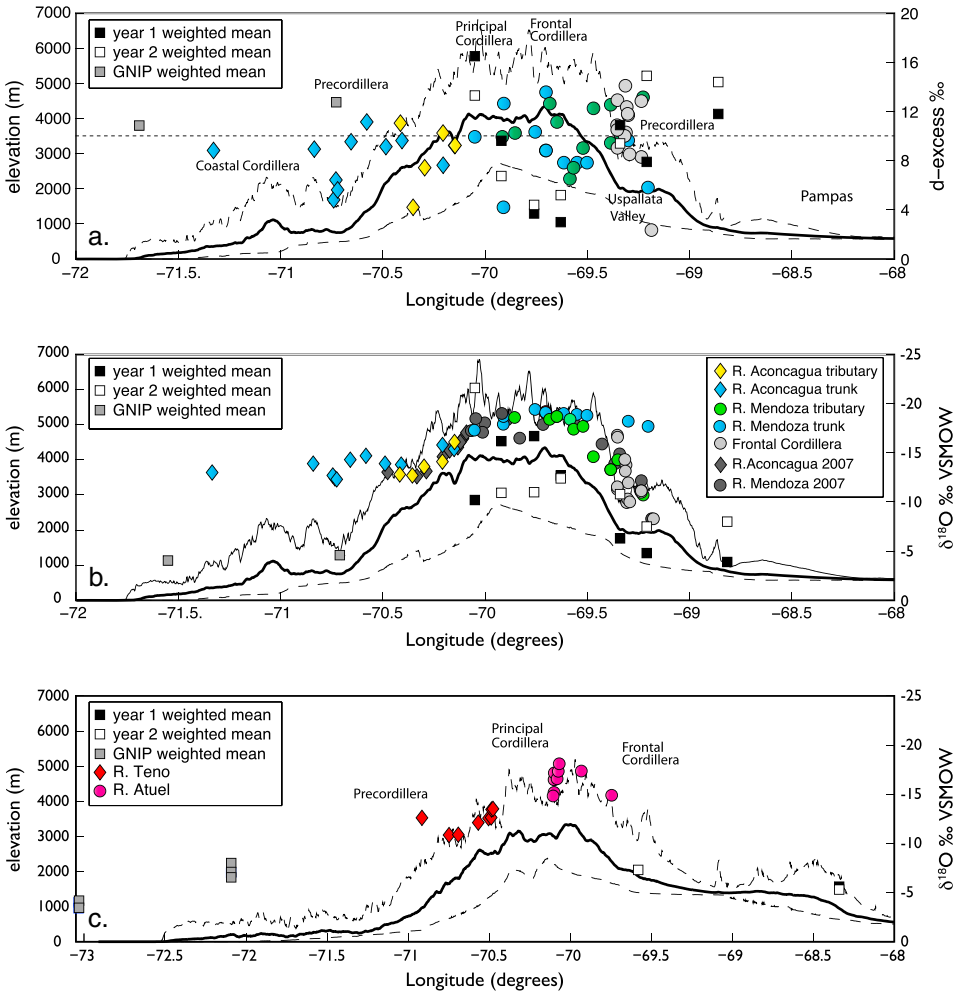

Figure 3. (a) Precipitation-weighted mean deuterium excess (d-excess) values for GNIP stations (gray boxes) in Chile, river water samples from small tributaries (diamonds and circles), and precipitation samples (boxes) versus station latitude. Black and white boxes correspond to d-excess weighted means for sample years 1 and 2, respectively. Topographic variation shown as minimum, maximum, and average elevation for the 100 km wide swath centered at 33°S (red box in Figure 1). Deuterium excess values in rivers and precipitation have a minimum in the frontal Cordillera. (b) Stream water, precipitation-weighted means from this study and GNIP weighted mean $\delta^{18}O$ values versus collection point or precipitation station latitude for the northern study area. Topographic profile is the same as in Figure 3a. (c) 100 km wide swath topographic profile centered at 35 °S (Figure 1) with $\delta^{18}O$ values for GNIP weighed mean precipitation values, weighted mean precipitation data from this study, and stream water versus sample collection latitude or station latitude.

of Chile and the western flank of the Andes between 32.5° and 35.5° is minor (<50 mm; Figure 2c). In contrast, winter precipitation reaches 300–400 mm in the lowlands of Chile, increases to 700–800 mm in valleys over the windward slope of the range, and sharply decreases east of the crest. Precipitation amount decreases from 200–300 mm in river valleys immediately east of the crest to less than 50 mm in Uspallata Valley and adjacent low lands of Argentina (Figure 1c). On the eastern flank of the Frontal Cordillera, the Precordillera, and in the adjacent lowlands of Argentina, the average summer precipitation regime of 150–200 mm is typically produced by orogenic-synoptic convective storms (Figure 1c), which are linked to northerly and easterly low-level winds that carry moisture from Atlantic and Amazon source regions.

[9] The quasi-decadal El Niño Southern Oscillation (ENSO) has a pronounced impact on modern-day climate over much of South America [*Garreaud et al.*, 2009], and an ENSO-like condition has been proposed for the Pliocene [*Wara et al.*, 2005]. In our study area, El Niño strengthens baroclinic activity at subtropical latitudes, which results in increased precipitation in the high Andes and the

western flanks of the range in Chile, yet this effect is directly mirrored by enhanced easterly circulation during La Niña events [*Montecinos et al.*, 2000]. While an El Niño event occurred from austral winter 2009 to austral autumn 2010, which is within the last 3 months of sampling year 1 and the first 6 months of sampling year 2, our 2 year sampling, and the lack on temporal continuity of GNIP stations make it difficult to explore the influence of El Niño or La Niña on our precipitation records.

3. Data and Methods

3.1. Precipitation Sampling

[10] Precipitation samples were collected in two geographic areas, at ~33°S and ~35°S (Figures 1b and 3). In each area, sample collectors were deployed at or near meteorological stations in order to obtain data on other climatic variables, in particular precipitation amount. The northern transect, consisting of seven stations spanning 2400 m of relief starts at the city of Mendoza (827 m) and extends to the border with Chile at Las Cuevas (3200 m; Figures 1b and 3a). The two southern stations are located at Malargüe (1400 m) and San Rafael (700 m).

[11] The precipitation collectors comprise a 2.5 cm opaque plastic pipe, 1 m in length, threaded endcaps, and a 2.5 to 5 cm coupling. The endcap and coupling were sealed in place with pipe adhesive. Upon deployment, collectors were filled with either light machine oil or lightweight motor oil to prevent sample evaporation between collections. Stations in the northern area were deployed in August of 2008 at Mendoza and in the Río Mendoza Valley. Sample collection in the south at Malargüe and San Rafael began in January of 2009. Every attempt was made to collect samples on a monthly basis; however, inclement weather or lack of personnel or a vehicle for collecting the samples occasionally hampered our efforts. At the end of the sample collection period in late 2010, a total of 18 attempts to recover precipitation were made in the northern area. Sampling in Malargüe and San Rafael was less frequent. (see Table 1 for station locations, elevations, and supplementary data for complete isotopic results).

3.2. River Water Sampling

[12] Isotopic data were collected from river waters in four catchments that drain the Andes between 35.5°S and 32.5°S. The Mendoza and Atuel Rivers drain the eastern flanks, and the Teno and Aconcagua Rivers the western (Figure 1). The Aconcagua and Mendoza River samples consist of previously unpublished δD and $\delta^{18}O$ data from 45 samples collected in the austral winter of 2002 from the

Table 1. Precipitation Sampling Station Elevations, Locations, Precipitation Amount, and Weighted Mean Isotopic Values

Station	Elevation (m)	Longitude (deg)	Latitude (deg)	Sampling Year	Samples Recovered	Total Precipitation (mm)	Weighted Means δD (VSMOW)	Weighted Means $\delta^{18}O$ (VSMOW)	Weighted Means d-excess
Las Cuevas	3200	−70.05	−32.81	1	10	549[a]	−65.0	−10.2	16.5
				2	7	795[a]	−159.3	−21.6	13.3
Puente del Inca	2750	−69.92	−32.82	1	6	175*	−123.5	−16.3	6.6
				2	4	170*	−82.6	−11.5	9.3
Punta de Vacas	2500	−69.76	−32.85	1	6	125	−129.7	−16.7	3.7
				2	3	119	−83.7	−11.0	4.4
Polvaredas	2250	−69.63	−32.78	1	6	113	−98.6	−12.7	3.0
				2	4	85	−93.8	−12.4	5.2
Uspallata	1900	−69.34	−32.58	1	7	83	−39.8	−6.3	10.9
				2	7	64	−76.9	−10.8	9.4
Potrerillos	1400	−69.21	−32.95	1	8	147	−30.7	−4.8	7.9
				2	6	64	−45.2	−7.5	14.9
Mendoza	827	−68.86	−32.89	1	8	180	−19.5	−3.9	11.8
				2	6	119	−50.0	−8.0	14.4
CNEA San Rafael	750	−68.34	−34.62	1	3	562	−39.3	−5.6	5.8
				2	9	628	−30.5	−5.3	12.3
Malargüe	1400	−69.58	−35.47	2	4	263	−46.0	−7.3	12.1

[a]Calculated from snow pillow data at El Portillo (Chile) using the transfer function determined in *Viale and Nuñez* [2011].
*Calculated from a transfer function of 1.4× precipitation at Punta de Vacas using the transfer function determined in *Viale and Nuñez* [2011].

trunk rivers and accessible tributaries which contained flowing water. All samples were filtered through a 0.45 micron filter with a syringe and collected in 30 mL high-density polyethylene bottles sealed with electrical tape. A total of 14 river water samples were collected from along the eastern flank of the Frontal Cordillera within the Mendoza River catchment but south of the trunk stream during Austral winter of 2007. Near 35°S, 22 samples were collected from tributaries of the Atuel River and Teno Rivers in 2007 during the austral summer and fall, respectively. In addition, we utilize previously published δD and $\delta^{18}O$ data from samples collected in the Aconcagua and Mendoza Rivers in austral summer of 2007 [*Hoke et al.*, 2009]. All 2007 samples were collected from tributaries with upstream areas between 5 and 100 km^2; these were collected in 15 mL centrifuge tubes whose threads were sealed with polytetrafluorethylene tape and caps wrapped with electrical tape to prevent sample loss. All samples were refrigerated prior to analysis. Mean catchment elevation for each sample was scaled to the mean elevation upstream of the collection point using an elevation weighted flow accumulation grid created in GIS.

3.3. Analytical Methods

[13] All water samples in this study were analyzed at the University of Rochester or at the University of Kentucky stable isotope laboratories. Precipitation samples and the 2002 river waters were analyzed using cavity ring-down spectrometery on either Los Gatos Research (Rochester) or Picarro (Kentucky) isotope analyzers. Standardization was based on measurements of VSMOW (Vienna Standard Mean Ocean Water) and GISP (Greenland Ice Sheet Precipitation). Analytical precision based on the repeated analysis of the internal standard is ±2.7‰ (1σ) for δD and ±0.3‰ (1σ) for $\delta^{18}O$, unless otherwise noted. The 2007 Frontal Cordillera stream analyses were run on a Thermo Electron Corporation Finnegan Delta plus XP mass spectrometer in continuous-flow mode via the Costech TC/EA peripheral and a GC-PAL autosampler. The 2σ uncertainties of hydrogen and oxygen isotopic results are 2.4‰ and 0.20‰, respectively, unless otherwise indicated.

3.4. Precipitation Amounts at Each Station

[14] The annual precipitation-weighted means for δD and $\delta^{18}O$ were calculated using the precipitation amounts from the meteorological station nearest each sample site. In most cases, sample collectors were deployed or within 1 km of the meteorological stations. Precipitation data are from either NOAA's Global Summary of the Day database (http://www7.ncdc.noaa.gov/CDO/cdo; [*NOAA*, 2012]), Subsecretaría de Recursos Hídricos (Sub-Secretary of Water Resources) [*SRH*, 2012], or Servicio Meteorológico Nacional (National Weather Service) of Argentina. Meteorological station precipitation data are not available for the sampling years at Las Cuevas or Puente del Inca. The station with precipitation data nearest Las Cuevas is the El Portillo snow pillow, located 7 km to the west in Chile and maintained by the Chilean Dirección General de Aguas (Figure 3a). Snow pillows use pressure to determine total water equivalent in millimeters above the pillow, with daily changes representing either melting (negative) or a snowfall event (positive). Snow pillows are generally deployed in locations where any impact from blowing snow is minimized. Using the transfer function for precipitation (P) of $P_{\text{Las Cuevas}} = 0.55 \times P_{\text{El Portillo}}$ from historical data [*Viale and Nuñez*, 2011], we estimate precipitation at Las Cuevas from the El Portillo snow pillow data. Puente del Inca does not have a weather station that measures precipitation amount; therefore we use a transfer function derived from *Viale and Nuñez* [2011] of $P_{\text{Puente del Inca}} = 1.4 \times P_{\text{Punta de Vacas}}$, which is close to the factor of ~1.5 times derived from a four-cell average of 4 km resolution Tropical Rainfall Measuring Mission (TRMM) data [*Bookhagen and Strecker*, 2008]. The absolute rainfall amount is less important than the relative magnitudes related to the seasonality of precipitation, and there is a strong linkage between storm events at El Portillo, Chile and Puente del Inca [*Viale and Nuñez*, 2011].

[15] In the area near 33°S, the seasonality of precipitation changes at Uspallata (Figure 2). To the east of Uspallata, precipitation is concentrated in the summer months (Mendoza in Figure 1c), while to the west, winter month precipitation dominates (Punta de Vacas in Figure 1c). Precipitation at Uspallata itself shows no strong seasonality (Uspallata in Figure 1c) with precipitation occurring throughout the year. Therefore, precipitation amount-weighted means east and west of Uspallata are strongly skewed according to the season of greatest precipitation. Precipitation in the southern area is dominated by austral summer rains in the plains of San Rafael. Malargüe, located at the foot of the Andes, has two precipitation maxima reflecting convective summer rain and winter spillover precipitation [*Viale and Nuñez*, 2011].

3.5. Rayleigh Fractionation Model

[16] In order to definitively discriminate between the precipitation moisture sources affecting the eastern slopes of the Andes between 32.5°S and 35.5°S, we explored a range of plausible scenarios using a Rayleigh fractionation model [*Rowley*, 2007; *Rowley et al*., 2001], which calculates the fractionation of oxygen with elevation for an air mass. The model considers the simple 1-D case of a single air mass fractionating as it rises and has no horizontal component [*Rowley*, 2007], nor does it consider moisture recycling or the effects of evapotranspiration, which may be important on the east side of the range. However, it can be applied to demonstrate how large or small deviations are from this simple, first-order approach. The general global case, as described by *Rowley* [2007], is applicable between 40°S and 40°N latitude. The model uses 2° × 2° grids of temperature (T) and relative humidity (RH) pairs from National Centers for Environmental Prediction (NCEP) reanalysis data to derive a probability density function of T and RH for the model. *Rowley et al*.'s [2001] original model used midlatitude Alpine GNIP stations to establish a 1500 m height above the surface for condensation, while *Rowley*'s [2007] revised model applied tropical GNIP data to attain a best-fit condensation height of 2000 m above the surface. The deviation between these models below 4000 m is small, and the weighted mean $\delta^{18}O$ values it calculates are nearly identical [*Rowley*, 2007]. Local conditions can be examined by specifying the shifts in RH and T from the global model. The range of parameter space in RH and T used to estimate the 1 and 2-sigma uncertainties is based on the probability density function derived from the RH and T pairs. The model is sensitive to assumptions about RH and T; however, in the case of orography, the effect of T is stronger than that of RH. Finally, the initial air mass $\delta^{18}O$ composition is derived from measurements at some relevant GNIP station and added to the change in $\delta^{18}O$ specified by the model.

[17] Between 32.5°S and 35.5°S, winter moisture is derived from the westerlies and summer moisture from easterlies of the low-level Andean Jet [*Vera et al*., 2006]. To test this hypothesis of source variability affecting the eastern Andean slopes at 33°S, we calculated initial starting conditions of RH and T for the following: (1) an austral winter air mass starting at Valparaiso, Chile; (2) an austral summer air mass starting at Mendoza, Argentina (Table 2). Average temperatures are calculated from meteorologic station data, and RH was taken from NCEP Reanalysis seasonal/monthly data composites (http://www.esrl.noaa.gov/psd/cgi-bin/data/composites/printpage.pl) for the relevant seasonal intervals over the 2 year period between September 2008 and September 2010 (Table 2). It is not necessary to explore the influences of large differences in RH, as the modest seasonal variations in relative humidity at Mendoza (<5%) and at Valparaiso (~20%) have minor impacts in the Rayleigh model relative that of temperature. $\delta^{18}O$ versus elevation are derived from appropriate seasonally or annually weighted means of GNIP data at Valparaiso and Mendoza. For the southern area (~35°S), we use RH and T and GNIP input values for austral winter conditions at Concepción, Chile and austral summer conditions at San Rafael (Figure 6c) with oxygen isotope values from this study.

Results

4.1. Isotopic Composition of Precipitation

[18] A total of 104 samples from the nine precipitation collectors were analyzed for δD and $\delta^{18}O$. The station with the highest number of samples is the Las Cuevas station ($n = 17$; location in Figure 1). All other stations were sampled less frequently. However, the $\delta^{18}O$ values for any sample reflect the sum of all rainfall between-sample collections unless the sample was lost for some reason such as brids trapped in the collectors (see auxiliary material); thus, weighted means are calculated using the appropriate total accumulation between collections. The local meteoric water line derived from all samples ($\delta D = 8.29\ \delta^{18}O + 11.75$; $R^2 = 0.98$) is indistinguishable from the global meteoric water line (GMWL) of *Rozanski et al*. [1993] and shifted slightly positive of the GMWL originally defined by *Craig* [1961]. When separated by sampling year (September to September), the LMWL shifts from $\delta D = 8.47\ \delta^{18}O + 14.2$

Table 2. Rayleigh Fractionation Modeling Parameters

Station	Season	Relative Humidity	Temperature (°C)	Initial $\delta^{18}O$ value
Mendoza	summer	55	25	−3.7 (GNIP)
Valparaiso	winter	88	12	−5.8 (GNIP)
San Rafael	summer	55	22	−5.5 (this study)
Concepción	winter	81	8.7	−4.1 (GNIP)

($R^2 = 0.99$) in year 1 to $\delta D = 7.91\ \delta^{18}O + 7.3$ ($R^2 = 0.96$) in year 2 (Figure 4a).

[19] Temperature changes throughout the year result in large variations in δ values at any given site, similar to that seen worldwide [*Rozanski and Araguás-Araguás*, 1995; *Rozanski et al.*, 1993]. The 3200 m Las Cuevas site has an arithmetic means of −93.5‰ and −12.8‰ with a range of 182‰ and 22‰ for δD and $\delta^{18}O$, respectively (Figure 5a). At lower elevation in the Andean foothills, the 1400 m Potrerillos site has an arithmetic means of −37.8‰ and −6.2‰, with range of 159‰ and 19‰ for δD and $\delta^{18}O$, respectively (Figure 4; Table 1 and auxiliary material Table 1).

[20] Precipitation amount-weighted δD and $\delta^{18}O$ for each collection site is calculated using the total precipitation for the sampling year and the amount of rainfall between-sample collections. These values exhibit interannual variation as high as 11.4‰ in δ18O at the Las Cuevas collection site; however, the average variation at all other sites is 4.3‰ (Figure 5a). As a whole, the 2 years of $\delta^{18}O$ data versus elevation exhibit a good fit ($r^2 = 0.7$, p-value <0.01) to the polynomial regression $z = -7.2(\delta^{18}O)^2 - 314.8(\delta^{18}O) - 367.6$ with standard errors of 4.7, 115.1, and 621.7, respectively (Figure 5b).

[21] Deuterium excess (d-excess; [*Dansgaard*, 1964]) is defined as d-excess = $\delta D - 8 * \delta^{18}O$. d-excess values of 10‰ reflect fractionation along the GMWL. Greater d-excess values indicate the addition or recycling of moisture from distinct sources [*Frölich et al.*, 2002; *Gat and Matsui*, 1991; *Kendall and Coplen*, 2001] and/or kinetic fractionation during snow formation and growth under oversaturated vapor conditions at temperatures below zero [*Jouzel and Merlivat*, 1984]. Vegetation and evapotranspiration also influence d-excess values [*Moreira et al.*, 1997; *Worden et al.*, 2007]. Lower d-excess values indicate subcloud evaporation [*Pang et al.*, 2011; *Stewart*, 1975]. Here, we calculate d-excess values from the precipitation amount-weighted δD and $\delta^{18}O$ values at each site for each sample year (Table 1), which range between 3‰ and 16‰.

[22] By adding d-excess values from the Santiago and Valparaiso GNIP stations, it is possible to examine the spatial variability in the d-excess values of precipitation across the Andes at 33°S (Figure 3a). The majority of weighted mean d-excess values (10 of 17) are ≥10‰, with four of the nine stations exhibiting consistently high d-excess, three stations exhibiting mixed signals, and two stations, Punta de Vacas and Polvaredas, consistently having values ≤5.2‰ (Figure 3a).

4.2. River Waters

[23] The δD and $\delta^{18}O$ values of 41 river water samples analyzed from the 2002 sampling of the Mendoza and Aconcagua Rivers range between −144.8 and −72.1‰ VSMOW and from −19.2 to −10.7‰ VSMOW, respectively. (Figure 3b). The 18 samples collected in austral winter of 2007 from small streams draining the flanks of the Frontal Cordillera have δD and $\delta^{18}O$ values ranging from −123.6 to −63.9‰ and −16.8 to −8.3‰, respectively (Figure 3b). d-excess values from rivers on

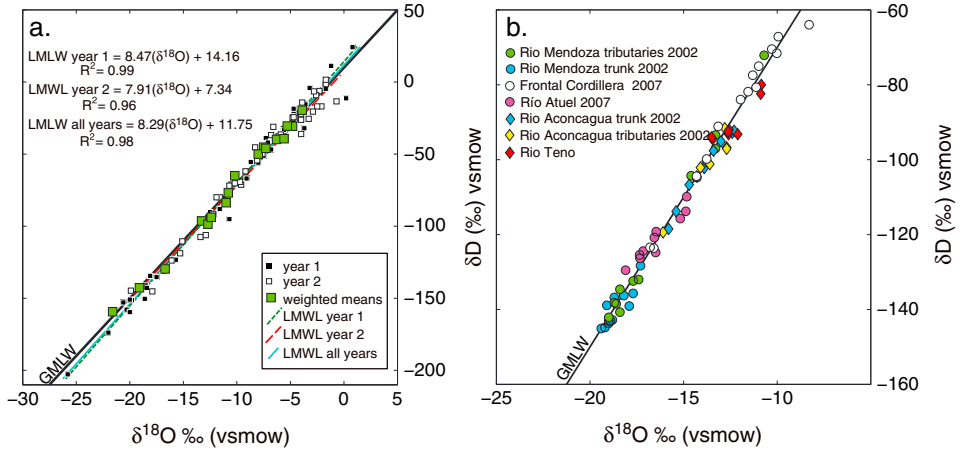

Figure 4. (a) $\delta^{18}O$ versus δD for individual precipitation samples and precipitation amount-weighted means for the 2 years of monthly precipitation sample collection. The global meteoric water line (GMWL) is plotted for reference, as are local meteoric water lines for sample year 1, sample year 2, and the combined dataset. (b) $\delta^{18}O$ versus δD for all river water samples analyzed as part of the study. The GMWL is shown for reference.

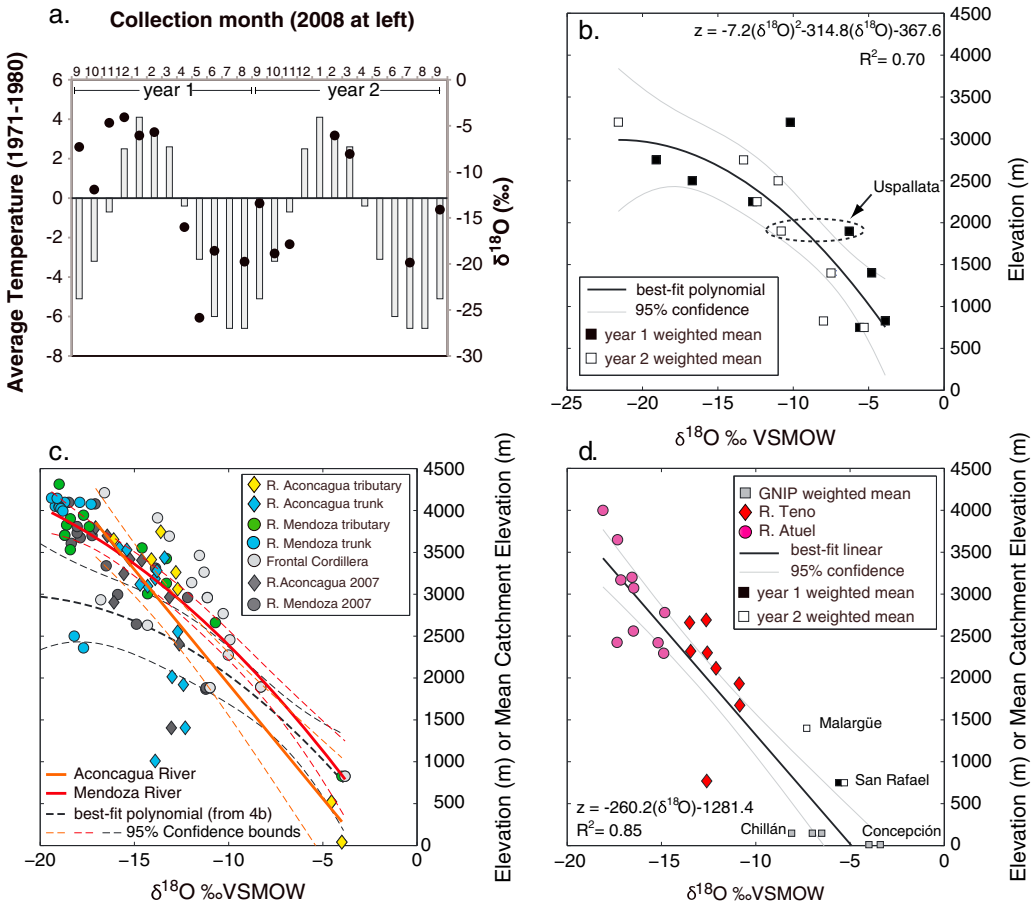

Figure 5. (a) Average monthly temperature at Las Cuevas based on long-term station data and the isotopic composition of precipitation for each sampling month between September 2008 and September 2010. (b) Plot of the weighted means of precipitation for each sample year (periods September to September starting in 2008) for the precipitation sampling stations in the Mendoza River catchment (Figure 1b). The best-fit least squares polynomial regression to all data and corresponding 95% confidence interval on the regression are shown by black and gray lines, respectively. (c) The isotopic compositions of river water samples in the northern study area near 33°S versus mean basin elevation upstream of the sampling point (hypsometric mean). All data from Chile and Argentina are represented by diamond and circle symbols, respectively. The thick dashed black line is the best-fit polynomial and associated 95% confidence bounds for precipitation from Figure 5b. The heavy red line and dashed red lines are the best-fit polynomial regression ($z = -5.8(\delta^{18}O)^2 - 339.7(\delta^{18}O) - 422.6$) through data from the small tributaries (drainage area $\leq 100\,km^2$) of the Mendoza River and associated 95% confidence interval, respectively. The orange line ($z = -273.5(\delta^{18}O) + 807$) represents the best fit for all of the small tributaries (drainage area $\leq 100\,km^2$) of the Aconcagua River. (d) The isotopic composition of Teno (red diamonds) and Atuel (mauve circles) Rivers versus mean basin elevation upstream of the water sampling point (hypsometric mean) and best-fit linear regression $z = -260.2(\delta^{18}O) + 1281$. Data from opposite sides of the range are pooled together because of the close proximity of the Atuel River samples to the drainage divide (Argentina-Chile border).

both sides of the range are between 2 and 15‰ VSMOW (Figure 3a). In addition to the new data presented here, we include the $\delta^{18}O$ data from the 2007 Mendoza and Aconcagua River transect presented in *Hoke et al.* [2009] in a statistical analysis of isotope-elevation trends.

[24] Following the approach of *Hoke et al.* [2009], we combine low elevation annual amount-weighted mean data from GNIP stations below 1000 m to derive linear or quadratic least squares regressions describing $\delta^{18}O$ versus mean basin elevation (Figure 5c). We also performed Chow tests [*Chow*, 1960], which provide an objective criteria for assessing whether or not different datasets are best explained a single or separate regression models. In this model, the null hypothesis is that the data are separate. To perform the test, a matrix with columns containing the $\delta^{18}O$ values from each dataset,

a column with a response variable (R) of 1 is assigned to one dataset, while the other is assigned 0, and a final column is the product of R and the $\delta^{18}O$ value ($R \times \delta^{18}O$). The linear system is solved using the vector containing the elevations for each dataset. The F-test statistic of R and $R \times \delta^{18}O$ yields a p-value, which is used to evaluate whether the regressions are independent (null hypothesis is correct, $p < 0.05$) or coincident ($p > 0.05$).

[25] The 2002 Mendoza River sample suite ($n = 24$) is from tributary and trunk streams. The trunk stream samples ($n = 12$), spanning nearly 2 km of mean basin elevation have an average δ18O value of -18.6 ± 0.7‰. Tributary samples from the 2002 sampling suite exhibit an 8.3‰ range in $\delta^{18}O$ values over a similar range of mean basin elevations, with the best-fit linear regression of $z = -215.2(\delta^{18}O) + 326$ ($r^2 = 0.91$, $p < 0.01$). The standard errors of the regression coefficients are 16.6 m and 271 m, respectively. The 2007 Frontal Cordillera samples reflect a range of 2.3 km in mean basin elevation with an 8.3‰ range in $\delta^{18}O$ values. The best-fit linear regression has the equation $z = -193.4(\delta^{18}O) + 408$ ($r^2 = 0.62$, $p < 0.01$). The standard errors of the regression coefficients are 46.5 m and 557 m, respectively. A Chow test of these regressions yields a p-value of 0.87; thus, we conclude that the regressions models are coincident. We then evaluate the coincidence of the 2007 Mendoza river data set with our combined Frontal Cordillera and 2002 Mendoza River dataset using another Chow test, which yields a p-value of 0.12 and confirms the coincidence of the regression models. We combine all three northern area datasets and derive the quadratic regression model $z = -5.8(\delta^{18}O)^2 - 339.7(\delta^{18}O) - 422.6$ (Figure 5c; $r^2 = 0.81$, $p << 0.01$). When applied to the 2007 and 2002 Aconcagua rivers tributary datasets, the Chow test yields a p-value of 0.87; thus, we conclude that regressions are coincident and that the data are best described in a common linear regression of $z = -273.5(\delta^{18}O) + 807$ ($r^2 = 0.81$, $p << 0.01$; Figure 5c). The standard errors of the regression coefficients are 35.6 m and 492 m, respectively.

[26] Samples from the Atuel and Teno Rivers ($n =$ between 35.5°S and 36°S) have δD values between −126.3 and −79.9‰, and $\delta^{18}O$ values range from −17.3 to −10.9‰ (Figure 4d). A Chow test on the coincidence of regressions on these rivers shows that they are coincident (p-value = 0.58); thus, we combine the data from these two rivers. Together, with the GNIP station data at Chillán and Concepción, the best-fit linear regression through the Atuel and Teno River data is linear and described by $z = -260.2(\delta^{18}O) + 1281$ ($r^2 = 0.85$, $p < 0.01$). The standard errors of the regression coefficients are 24.0 m and 320.7 m, respectively (Figure 5d).

4.3. Rayleigh Fractionation Model

[27] In order to evaluate changes in water isotope compositions that should result from the ascent of Atlantic and Pacific air masses over the Andes, we employ a series of Rayleigh fractionation models (Figure 6 and Table 2). Using GNIP and atmospheric data from Chilean and Argentine stations (see section 3.5) to constrain the isotopic composition of initial (low elevation) air mass vapor, we are able to explore the average annual and seasonal differences in $\delta^{18}O$ lapse rates on both sides of the range. In the northern area, differences in the modeled values of $\delta^{18}O$ on the western slope (winter) and eastern slope (summer) exhibit no significant overlap, suggesting that such an approach accurately differentiates summer and winter moisture sources in the precipitation amount-weighted means (Figure 6a). When weighted mean precipitation composition data are plotted relative to the model outputs (Figure 6a), it becomes apparent that, with the exception of the Las Cuevas site (which falls within the eastern, Argentine austral summer field), all high elevation (>2 km) collection sites from year 1 fall within confidence intervals for Chilean (western, austral winter moisture source) model results (Figure 6a). Below 2 km elevation, year 1 data are mostly within the Argentine model results. Weighted mean isotopic compositions from sample year 2 either fall within the Chilean fractionation model or fall between the Argentine and Chilean fractionation models (Figure 6a).

[28] Because of the dominance of the westerlies on the western flanks of the Andes and the geographic position of the Atuel River samples in the core of the range, in the southern study area, we restrict our modeling to the winter and summer average fraction curves using the weighted mean isotopic values from the Concepción, Chile GNIP station along with winter T and RH estimated from Chilean Weather Service data. River data mostly plot along the modeled weighted mean curve or within the 2σ bounds of the model (Figure 6c). The isotopic compositions of our Malargüe and San Rafael, Argentina stations as well as the Chillán, Chile GNIP station are plotted in Figure 6c for comparison.

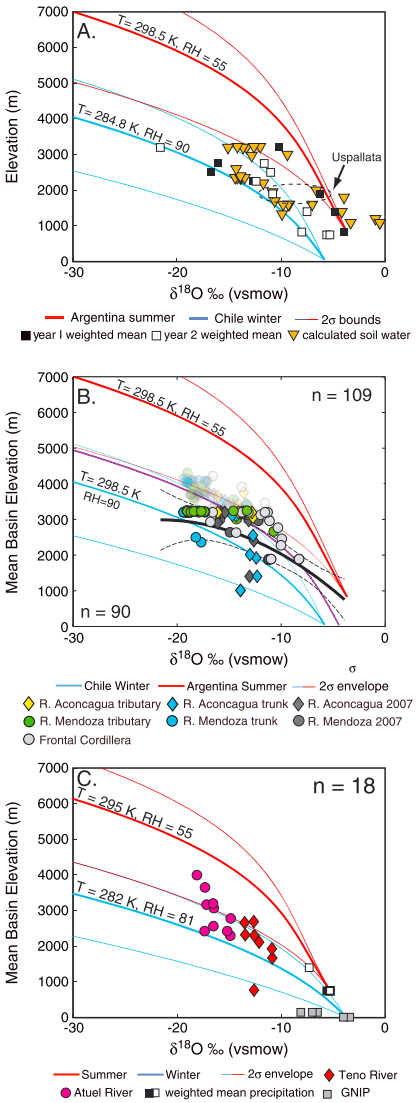

Figure 6. (a) Rayleigh fractionation model results for argentine summer and Chilean winter (see Table 2) with isotopic values from precipitation-weighted means (squares) and temperature-corrected estimates of soil water from pedogenic carbonates (circles). Models use starting conditions reflecting the elevation, temperature, and relative humidity at Valparaiso, Chile, and Mendoza, Argentina. (b) The same Rayleigh fractionation models as Figure 6a, plotted with river water $\delta^{18}O$ values from the Aconcagua River (diamonds) and Mendoza River (circles). Faded symbols represent the hypsometric mean elevations of river water samples >3200 m in elevation, which have been shifted to an effective elevation of 3200 m based on the observed ceiling in $\delta^{18}O$ values observed in Figure 5b. (c) Model results for winter conditions for an air mass at Concepción, Chile and summer conditions at San Rafael, Argentina plotted with river waters from the Atuel and Teno Rivers and weighted mean precipitation values for San Rafael and Malargüe (see Table 2). River water data reflects a dominance of a winter moisture source for river waters.

5. Discussion

[29] Our study combines several data sets to present a complete view of the moisture sources for precipitation and isotopes in precipitation, rivers, and pedogenic carbonates on the eastern flanks of the Andes in the subtropical latitudes. While our study is in the Andes, the inferences we draw from these data are relevant globally for studies that examine atmospheric, hydrologic, and geologic relations in and adjacent to mountain ranges.

5.1. Discrimination of Source Regions in Precipitation

[30] Our 2 years of data, when evaluated with the Rayleigh fractionation models, capture the potential significance of interannual variation in the spillover of Pacific-sourced moisture on the eastern flanks of the Andes (Figure 6a). Year 1 precipitation data (black squares in Figure 6a) shows a strong "eastern slope" signal at low elevations and a mixed signal at higher elevations. The isotopic composition of precipitation in year 2 (open squares in Figure 6a) falls entirely outside the range of values for Argentine (summer) conditions predicted by the Rayleigh model, with values either within the Chilean (winter) model or a mixed signal between the models in Figure 6a. In general, the geographic position of Uspallata (Figure 1c) represents an \important boundary between moisture sources based on the lack of seasonality at this site in precipitation and the observation that above Uspallata the isotopic composition or precipitation is more heavily weighted towards winter moisture sources (Figure 6a).

5.2. Spatial Pattern of d-Excess

[31] The majority of weighted mean d-excess values for the precipitation collection sites in the Mendoza River valley and the GNIP station in Chile have values ≥10‰ (Figure 3a). This indicates vapor recycling, or that the air mass is recharged by different potential processes during its ascent of the range [e.g., *Bershaw et al.*, 2012; *Kendall and Coplen*, 2001; *Koster et al.*, 1993]. Given the observation of high d-excess values at Mendoza in the lowlands at the foot of the range (Figure 5a), it is difficult to determine whether increased d-excess is from moisture recycling prior to the arrival of the air mass at the foot of the range or during its ascent. However, potential recycling or recharge processes, which may account for high d-excess at high altitude locations, include the following: (1) evaporation from the warm surface

during convective summer precipitation in the eastern plains derived from either the low-level Andean Jet or the Atlantic; (2) the "seeder-feeder" process, which is typically responsible for orographic precipitation enhancement over the upslope of the ranges [e.g., *Houze*, 2012; *Roe*, 2005]; and (3) kinetic fractionation in a mixed phase environment where snow grows with water migrating from liquid to vapor and then snow.

[32] The minimum in weighted mean precipitation d-excess values between 3‰ and 5.2‰ are spatially confined to a specific <30 km geographic area in the western half of the Frontal Cordillera (Polaveradas and Punta de Vacas; Figures 1 and 3a). Monthly d-excess values at these stations are consistently lower than those at surrounding stations during both sampling years. This d-excess minimum corresponds to the boundary between winter (western) and summer (eastern) precipitation regimes observed by *Viale and Nuñez* [2011] and likely marks the western extent of Atlantic precipitation. Remarkably, d-excess values from rivers also show a pronounced minimum in the same geographic regions (Figure 3a), reflecting preservation of the signal between meteoric and surface waters. Low d-excess values are interpreted to indicate subcloud evaporation of precipitation [*Stewart*, 1975]. We attribute the persistent geographically isolated low in d-excess observed in our data to downslope flow (Föhen winds, locally called Zonda wind) during precipitation events, which favor greater subcloud evaporation in this part of the Mendoza River Valley.

5.3. Precipitation to Rivers

[33] In general, surface waters sampled from small catchments are thought to accurately reflect the time-integrated $\delta^{18}O$ of precipitation [e.g., *Hren et al*., 2009; *Rowley and Garzione*, 2007]. Incorporating data from *Hoke et al*.'s [2009] sample suite, collected in the austral summer of 2007, with our new results allows us to explore the potential for variation in the integration of isotopic signals over subdecadal timescales. Our statistical analysis finds no significant difference in river waters over the 5-year period between samplings on either side of the range. In the northern study area at 33°S, the isotopic compositions of river waters on both flanks of the range diverge from precipitation at elevations >2.4 km (Figures 3b). However, when examined in the context of the spatial and topographic structure of the range (Figure 3b), it is clear that an apparent limit to $\delta^{18}O$ values exists, which corresponds spatially with the area where the mean range elevation is ~4 km. We interpret the limit in $\delta^{18}O$ values to indicate the cessation of air mass ascent across the range. This is indicated by the sharp increase in $\delta^{18}O$ values over a very short horizontal distance, coincident with the flanks of the range, although the lower density and smaller elevation range from samples makes this trend less apparent in Chile (Figure 3b). The trunk streams are dominated by the high elevation recharge on both flanks of the range (Figures 3b and 5c); a pattern documented by the $\delta^{18}O$ values of groundwater wells in the lowlands of the Mendoza River watershed [*Panarello and Dapeña*, 1996]. The best-fit regression through our weighed mean precipitation data has a zero slope at a $\delta^{18}O$ value of −21.6‰ and 3200 elevation, while river data reach their $\delta^{18}O$ ceiling at ~−18‰, but ~1 km higher in terms of mean basin elevation above the location where the sample was collected. The limit implies that between the flanks of the range, rivers $\delta^{18}O$ values are insensitive to their mean hypsometric elevation once the air mass reaches its maximum level of ascent as it crosses the range, which artificially exaggerates the isotope-elevation gradient observed in rivers. d-excess values of <10‰ from 28 of the 59 river water samples indicate pervasive evaporative enrichment of surface waters on both sides of the range (Figure 3a), which may result in the discrepancy between maximum $\delta^{18}O$ values in rivers and the maximum precipitation $\delta^{18}O$ value from Las Cuevas. However, because low d-excess is not consistent across all rivers, yet all share the same $\delta^{18}O$ values, we interpret evaporation to have only a minor factor in the observed $\delta^{18}O$ limit. If we took all river water data with mean basin elevations >3200 m and applied a similar elevation ceiling, it would improve the coincidence of the rivers with precipitation data and the winter Rayleigh fractionation curve (Figure 6b).

[34] Comparison of precipitation and river water $\delta^{18}O$ values in the southern region at ~35°S combines 1 year of river samples, GNIP data from two stations in Chile, and two precipitation stations in Argentina. At this latitude, the range has a simple, well-defined range crest (Figure 3c). The $\delta^{18}O$ of river waters are close to those predicted by fractionation models incorporating winter conditions for an air mass starting at Concepción, Chile. This suggests a strong dominance of western, winter precipitation in the southern area (~35°S). The dominance of low d-excess values in the Teno River (Figure 5; Table 3 in the auxiliary material), records the evaporative enrichment of

surface waters, making $\delta^{18}O$ values from river waters maximum values of the weighted mean isotopic composition of the original precipitation. Together, these results suggest that river waters near 35°S yield isotopic values which largely reflect mean winter to mean annual conditions.

[35] The sharp transition we observe from mixed precipitation sources at 33°S to a pure winter signal at 35°S is consistent with previous climatological studies in the region [*Viale and Nuñez*, 2011]. This can be attributed to increased storm frequency towards the south coupled with the lower average elevation of the Andes at 35°S, enabling more westerly spillover precipitation. Caution must be exercised when extrapolating isotope-elevation relationships or when inferring the seasonality and source of precipitation in high mountain ranges such as the Andes.

5.4. Meteoric Precipitation, River Water, and Authigenic Carbonates

[36] Models predicting the seasonal and interannual variability in the isotopic composition of precipitation have been used to cast doubt on the utility of interpreting the $\delta^{18}O$ values of pedogenic carbonates as accurate records of time-averaged conditions [*Jeffery et al.*, 2012]. In addition, it is important to determine whether isotope-elevation relationships derived from rivers do indeed serve as accurate proxies for the weighted mean precipitation as assumed in most paleoaltimetry studies; this is especially important for the application of paleoaltimetry to relatively narrow, nonplateau mountain ranges. To explore these issues, we compare soil water $\delta^{18}O$ values calculated from Latest Pleistocene to Holocene pedogenic carbonate samples collected in the Mendoza River valley (Figure 7) [*Hoke et al.*, 2009; *Peters et al.*, 2013]. The ages of the pedogenic carbonates sampled in these studies are constrained by stratigraphic relationships to glacial deposits and other deposits of known age [*Hoke et al.*, 2009, *Peters et al.*, 2013].

[37] The original calculation of soil water $\delta^{18}O$ values presented by *Hoke et al.* [2009] used the empirical fractionation factor calculation from *Kim and O'Neil* [1997] with the assumption that the soil temperature at the time of carbonate formation reflected mean annual air temperatures. Subsequent Δ_{47} 'clumped isotope' carbonate thermometer work in Argentina by *Peters et al.* [in press] demonstrates that average soil temperatures are 5–15°C higher than those assumed by *Hoke et al.* [2009] at elevations above 1600 m. Here, we use the clumped isotope corrected soil water calculations from *Peters et al.* [in press], which include recalculations of soil waters from *Hoke et al.*'s [2009] data and new soil water $\delta^{18}O$ values from pedogenic carbonates in Argentina (Figures 6 and 7). Pedogenic carbonate $\delta^{18}O$ values, like those of weighted mean precipitation, fall within and between the range of solutions predicted by end-member summer and winter Rayleigh fractionation models (Figure 6a). The correspondence of calculated soil water with our 2 year record of precipitation is remarkable, if not troubling, as it challenges the commonly held assumption that the soil water used in carbonate formation mirrors the weighted mean average of meteoric waters [*Cerling and Quade*, 1993]. Only five calculated soil water $\delta^{18}O$ values fall outside the 2-sigma values predicted by the summer conditions Rayleigh fractionation model (Figure 6a). We interpret the values that lie to the right (more positive $\delta^{18}O$ values) of the summer curve in Figure 6a to reflect evaporative enrichment of the soil water in ^{18}O. This indicates that soil carbonates may not be the great averaging agent they are commonly assumed to be, instead they are capable of capturing the range of variations in precipitation, perhaps reflecting (1) stochastic nature of precipitation in arid environments or (2) a strong seasonal bias in carbonate formation [*Breecker et al.*, 2009; *Peters et al.*, 2013]. Between elevations of 2700 m and 1300 m, several calculated soil waters have $\delta^{18}O$ values lie wholly within the winter precipitation field, while other samples within

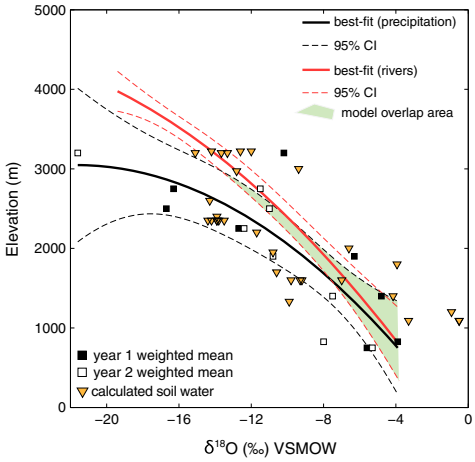

Figure 7. Best-fit curves and 1-sigma uncertainties of $\delta^{18}O$ versus elevation for weighted mean precipitation and all river tributary data from the Mendoza and Aconcagua River valleys. Calculated soil water isotopic compositions and weighted mean precipitation data are plotted in circles and squares, respectively. The light green shaded area represents the overlap between the 1-sigma uncertainties

the same band of elevation have more positive $\delta^{18}O$ values. Based these data, we speculate that evaporative enrichment affects the samples with more positive $\delta^{18}O$ values and that using the most negative values may be the best estimate of the isotopic composition of soil waters, which have not experienced significant evaporative enrichment. Unfortunately, with our data we cannot quantify nor control for the spatial controls, if any, on the evaporative enrichment of the soil water as no direct measurements of modern soil water $\delta^{18}O$ data exist at these sites.

[38] With isotopic data on precipitation, river waters, and well-corrected soil water $\delta^{18}O$ calculations along the same elevation transect in the same valley, we can assess the ability of pedogenic carbonates to reflect isotope-elevation gradients from either rivers or precipitation. Figure 7 shows the best-fit curves derived from the tributaries of the Aconcagua and Mendoza Rivers (Figure 5c) and the weighted mean precipitation from Figure 5b. Calculated soil water isotopic compositions and undifferentiated weighted mean precipitation values are also shown in Figure 7. The best-fit line through the precipitation data represent an averaging of the spatial distribution of winter and summer precipitation on the eastern flank of the Andes. As discussed above, rivers diverge from precipitation at ~2400 m and define an isotope-elevation gradient which is steeper than that for precipitation. The area of overlap at the 1-sigma level is relatively narrow. Based on the 1-sigma bounds, calculated soil waters are a better overall match to the trend defined by precipitation rather than rivers (Figure 7). Application of the isotope-elevation gradient derived from rivers would increasingly overestimate elevations above 1600 m and increasingly underestimate elevations below. The geologic scenario of preserving pedogenic carbonate along an elevation transect such as that of the Río Mendoza Valley beyond 1 Ma is slim; however, our data show that reconstruction of a crude isotope-elevation curve, which reflects average precipitation values, is possible.

6. Conclusions

[39] This study demonstrates that precipitation on the eastern slopes of the Andes between 32.5°S and 35.5°S is isotopically differentiable into Pacific-sourced winter moisture and Atlantic/Amazonian-sourced summer moisture sources based on Rayleigh fractionation modeling. In northern Mendoza, west of the town of Uspallata, precipitation is dominated by Pacific winter moisture, while to the east year to year variability suggests interannual fluctuations in the reach of the westerly air mass over the range. Geographically isolated low d-excess values at two sample sites in the Mendoza River suggest significant subcloud evaporation of precipitation during downslope flow during precipitation events. River water data in the northern area are best fit to Rayleigh fraction models reflecting average annual conditions on both sides of the range. In the southern part of our study, rivers in Chile and Argentina are a best fit to conditions between winter and average annual Rayleigh fractionation models. Finally, a comparison of precipitation amount-weighted means from the eastern slopes of the Andes, rivers on both sides of the range at ~33°S, and soil water $\delta^{18}O$ values calculated from clumped isotope temperature-corrected pedogenic carbonates shows that soil waters capture the range of seasonality reflected in modern precipitation and to a lesser degree reflect the average signal of river waters. Soil carbonates are more representative of precipitation, and the use of river isotope-elevation gradients rates would tend to overestimate elevations at high elevations and underestimate at low elevations. Precipitation-based isotope-elevation gradients would lead to more accurate paleoelevation estimates.

Acknowledgments

[40] The Dirección de Recursos Naturales Renovables, division of Áreas Protegidas of the province of Mendoza provided permission to deploy collectors in protected areas, and park rangers (E. Rojas, A. Zalazar, O. Aranibar, R. Olivera, and M. García) helped with sample collection in remote sites. Ricardo Villalba's (IANIGLA) support allowed the use of institute equipment for this project and the collaboration of IANIGLA staff (E. Corvalán, M. Quiroga, H. Videla, J. Hernandez, S. Crespo, M. L. Gomez) in precipitation sample collection. E. Previtera was instrumental in the collection of the Teno and Atuel river water samples. P. Higgins and B. Hough (University of Rochester) handled sample analysis. We thank D.B. Rowley for permission to use his Rayleigh fractionation model. Discussions with and comments from B. H. Wilkinson during writing are gratefully acknowledged. We thank the two anonymous referees, one of whom provided a very thorough review, along with additional comments from Editor Louis Derry, which served to greatly strengthen this paper. This work was funded by NSF grant OISE-0601957 to Hoke.

References

Bershaw, J., S. M. Penny, and C. N. Garzione (2012), Stable isotopes of modern water across the Himalaya and eastern Tibetan Plateau: Implications for estimates of paleoelevation

and paleoclimate, *J. Geophys. Res.*, *117*(D2), D02110, doi:10.1029/2011JD016132.

Bookhagen, B., and M. R. Strecker (2008), Orographic barriers, high-resolution TRMM rainfall, and relief variations along the eastern Andes, *Geophys. Res. Lett.*, *35*, L06403, doi:10.1029/2007GL032011.

Bowen, G. J., and B. Wilkinson (2002), Spatial distribution of delta O-18 in meteoric precipitation, *Geology*, *30*(4), 315–318, doi:10.1130/0091-7613(2002)030<0315:SDOOIM>2.0.CO;2.

Breecker, D., Z. Sharp, and L. Mcfadden (2009), Seasonal bias in the formation and stable isotope composition of pedogenic carbonate in modern soils from central New Mexico, USA, *Geol. Soc. Am. Bull.*, *121*(3/4), 630–640, doi:10.1130/B26413.1.

Cerling, T. E., and J. Quade (1993), Stable carbon and oxygen isotopes in soil carbonates, in *Climate Change in Continental Isotopic Records*, edited by P. K. Swart, K. C. Lohmann, J. McKenzie and S. M. Savin, pp. 217–231, American Geophysical Union, Washington D.C, doi:10.1029/GM078p0217.

Chow, G. C. (1960), Tests of equality between sets of coefficients in two linear regressions, *Econometrica*, *28*(3), 591–605, doi:10.2307/1910133.

Craig, H. (1961), Isotopic variations in meteoric waters, *Science*, *133*(3465), 1702–1703.

Dansgaard, W. (1964), Stable isotopes in precipitation, *Tellus*, *16*, 436–468, doi:10.1111/j.2153-3490.1964.tb00181.x.

Ehlers, T. A., and C. J. Poulsen (2009), Influence of Andean uplift on climate and paleoaltimetry estimates, *Earth Planet. Sci. Lett.*, *281*(3-4), 238–248, doi:10.1016/J.Epsl.2009.02.026.

Ereño, C. E., and J. A. J. Hoffmann (1978), El regimen pluvial en la Cordillera Central, *Ser. Cuad Geogr. 5*, 1–17.

Frölich, K., J. J. Gibson, and P. Aggarwal (2002), Deuterium excess in precipitation and its climatological significance, paper presented at Study of Environmental Change using Isotope Techniques, IAEA, Vienna, Austria.

Garreaud, R. D., M. Vuille, R. Compagnucci, and J. Marengo (2009), Present-day South American climate, *Palaeogeogr. Palaeoclimatol.*, *281*, 180–195, doi:10.1016/j.palaeo.2007.10.032.

Garzione, C. N., J. Quade, P. G. DeCelles, and N. B. English (2000), Predicting paleoelevation of Tibet and the Himalaya from delta O-18 vs. altitude gradients in meteoric water across the Nepal Himalaya, *Earth Planet. Sci. Lett.*, *183*(1-2), 215–229, doi:10.1016/S0012-821X(00)00252-1.

Garzione, C. N., G. D. Hoke, J. C. Labarkin, S. Withers, B. J. MacFadden, P. Ghosh, and A. Mulch (2008), Rise of the Andes, *Science*, *320*, 1304–1307, doi:10.1126/science.1148615.

Gat, J., and E. Matsui (1991), Atmospheric water-balance in the Amazon Basin—An isotopic evapotranspiration model, *J Geophys. Res. Atmos.*, *96*(D7), 13179–13188, doi:10.1029/91JD00054.

Ghosh, P., C. N. Garzione, and J. M. Eiler (2006), Rapid uplift of the Altiplano revealed through C-13-O-18 bonds in paleosol carbonates, *Science*, *311*(5760), 511–515, doi:10.1126/science.1119365.

Gonfiantini, R., M. Roche, J. Olivry, J. Fontes, and G. Zuppi (2001), The altitude effect on the isotopic composition of tropical rains, *Chem. Geol.*, *181*(1-4), 147–167, http://dx.doi.org/10.1016/S0009-2541(01)00279-0.

Haselton, K., G. Hilley, and M. R. Strecker (2002), Average Pleistocene climatic patterns in the southern central Andes: Controls on mountain glaciation and paleoclimate implications, *J. Geol.*, *110*(2), 211–226, doi:10.1086/338414.

Hoffmann, J. A. J. (1975), Climatic atlas of South America, WMO; UNESCO, Geneva.

Hoke, G. D., C. N. Garzione, D. C. Araneo, C. Latorre, M. R. Strecker, and K. J. Williams (2009), The stable isotope altimeter: Do Quaternary pedogenic carbonates predict modern elevations?, *Geology*, *34*(11), doi:10.1130/G30308A.1.

Houze, R. A. J. (2012), Orographic effects on precipitating clouds, *Rev. Geophys.*, *50*, doi:10.1029/2011RG000365.

Hren, M. T., B. Bookhagen, P. M. Blisniuk, A. L. Booth, and C. P. Chamberlain (2009), delta O-18 and delta D of streamwaters across the Himalaya and Tibetan Plateau: Implications for moisture sources and paleoelevation reconstructions, *Earth Planet. Sci. Lett.*, *288*, 20–32, doi:10.1016/j.epsl.2009.08.041.

IAEA (2006), *Isotope Hydrology Information System.* The ISOHIS Database, edited, IAEA, Vienna.

Jeffery, M., C. Poulsen, and T. A. Ehlers (2012), Impacts of Cenozoic global cooling, surface uplift, and an inland seaway on South American paleoclimate and precipitation δ18O, *Geol. Soc. Am. Bull.*, *124*(7-8), 1027–1047, doi:10.1130/B30480.1.

Jouzel, J., and L. Merlivat (1984), Deuterium and oxygen 18 in precipitation: Modeling of the isotopic effects during snow formation, *J. Geophys. Res.*, *89*(D7), 11749–11711,11757, doi:10.1029/JD089iD07p11749.

Kendall, C., and T. Coplen (2001), Distribution of oxygen-18 and deuterium in river waters across the United States, *Hydrol. Processes*, *15*(7), 1363–1393, doi:10.1002/hyp.217.

Kim, S.-T., and J. R. O'Neil (1997), Equilibrium and nonequilibrium oxygen isotope effects in synthetic carbonates, *Geochim. Cosmochim. Acta*, *61*(16), 15, http://dx.doi.org/10.1016/S0016-7037(97)00169-5.

Kleinert, K., and M. R. Strecker (2001), Climate change in response to orographic barrier uplift: Paleosol and stable isotope evidence from the late Neogene Santa Maria basin, northwestern Argentina, *Geol. Soc. Am. Bull.*, *113*(6), 728–742, doi:10.1130/0016-7606(2001)113<0728:CCIRTO>2.0.CO;2.

Koster, R., D. Devalpine, and J. Jouzel (1993), Continental water recycling and (H2O)-O-18 concentrations, *Geophys. Res. Lett.*, *20*(20), 2215–2218, doi:10.1029/93GL01781.

Lamb, S. (2011), Did shortening in thick crust cause rapid Late Cenozoic uplift in the northern Bolivian Andes?, *J. Geol. Soc. London*, *168*(5), 1079–1092, doi:10.1144/0016-76492011-008.

Masiokas, M., R. Villalba, B. Luckman, C. Le Quesne, and J. Aravena (2006), Snowpack variations in the Central Andes of Argentina and Chile, 1951–2005: Large-scale atmospheric influences and implications for water resources in the region, *J. Climate*, *19*(24), 6334–6352, doi:10.1175/JCLI3969.1.

Miller, A. (1976), The Climate of Chile, in *World Survey of Climatology: Climates of Central and South America*, edited by W. Schwerdtfeger, pp. 113–145, Elsevier, Amsterdam.

Montecinos, A., A. Díaz, and P. Aceituno (2000), Seasonal diagnostic and predictability of rainfall in subtropical South America based on tropical Pacific SST, *J. Climate*, *13*(4), 746–758, doi:10.1175/1520-0442(2000)013<0746:SDAPOR>2.0.CO;2.

Moreira, M., L. Sternberg, L. Martinelli, R. Victoria, E. Barbosa, L. Bonates, and D. Nepstad (1997), Contribution of transpiration to forest ambient vapour based on isotopic measurements, *Glob. Chang. Biol.*, *3*(5), 439–450, doi:10.1046/j.1365-2486.1997.00082.x.

Mulch, A., S. A. Graham, and C. P. Chamberlain (2006), Hydrogen isotopes in Eocene river gravels and paleoelevation of

the Sierra Nevada, *Science*, *313*, 87–89, doi:10.1126/science.1125986.

NOAA (2012), NNDC Climate data online, in NOAA Satellite and Information Service, edited by Data and Information Service, National Environmental Satellite, National Oceanic and Atmospheric Administration, Washington, D.C. http://www7.ncdc.noaa.gov/CDO/cdo

Panarello, H. O., and C. Dapeña (1996), Mechanismos de recarga y salinizacion en las cuencas sedimentarias de los Rios Mendoza y Tunuyan, Mendoza, Republica Argentina: Evidenciados por isotopos ambientales, paper presented at XII Congreso Geologico de Bolivia, Sociedad Geologica Boliviana, Tirija, Bolivia, October 10-13 1996.

Pang, Z., Y. Kong, K. Froehlich, T. Huang, L. Yuan, Z. Li, and F. Wang (2011), Processes affecting isotopes in precipitation of an arid region, *Tellus B*, *63*(3), 352–359, doi:10.1111/j.1600-0889.2011.00532.x.

Peters, N. A., K. W. Huntington, and G. D. Hoke (2013), Hot or not? Impact of seasonally variable soil carbonate formation on paleotemperature and O-isotope records from clumped isotope thermometry, *Earth Planet Sc Lett*, *361* (C), 208–218, doi:10.1016/j.epsl.2012.10.024.

Polissar, P., K. Freeman, D. Rowley, F. McInerney, and B. Currie (2009), Paleoaltimetry of the Tibetan Plateau from D/H ratios of lipid biomarkers, *Earth Planet. Sci. Lett.*, *287* (1-2), 64–76, doi:10.1016/j.epsl.2009.07.037.

Prohaska, A. (1976), The climates of Uruguay, Argentina and Paraguay, in *World Survey of Climatology: Climates of Central and South America*, edited by W. Schwerdtfeger, pp. 12–112, Elsevier, Amsterdam.

Roe, G. H. (2005), Orographic precipitation, *Annu. Rev. Earth Pl. Sci.*, *33*, 645–671, doi:10.1146/annurev.earth.33.092203.122541.

Rowley, D. B. (2007), Stable isotope-based paleoaltimetry: Theory and validation, *Revi. Mineral. Geochem.*, *66*(1), 23–52, doi:10.2138/rmg.2007.66.2.

Rowley, D. B., and B. S. Currie (2006), Paleo-altimetry of the late Eocene to Miocene Lunpola basin, central Tibet, *Nature*, *439*, 677–681, doi:10.1038/nature04506.

Rowley, D. B., and C. N. Garzione (2007), Stable isotope-based paleoaltimetry, *Annu. Rev. Earth. Pl. Sci.*, *35*(1), 463–508, doi:10.1146/annurev.earth.35.031306.140155.

Rowley, D. B., R. T. Pierrehumbert, and B. S. Currie (2001), A new approach to stable isotope-based paleoaltimetry: Implications for paleoaltimetry and paleohypsometry of the High Himalaya since the Late Miocene, *Earth Planet. Sci. Lett.*, *188*(1-2), 253–268, doi:10.1016/S0012-821X(01)00324-7.

Rozanski, K., and L. Araguás-Araguás (1995), Spatial and temporal variability of stable isotope composition of precipitation over the South American continent, *Bull. Inst. Fr. Etudes Andines*, *24*(3), 379–390.

Rozanski, K., L. Araguás-Araguás, and R. Gonfiantini (1993), Isotopic patterns in modern global precipitation, *Geophys. Monogr. Ser.*, *78*, 1–36, doi:10.1029/GM078p0001.

Sauer, P. E., T. I. Eglinton, J. M. Hayes, A. Schimmelmann, and A. L. Sessions (2001), Compound-specific D/H ratios of lipid biomarkers from sediments as a proxy for environmental and climatic conditions, *Geochim. Cosmochim. Acta*, *65*(2), 213–222, doi:10.1016/S0016-7037(00)00520-2.

Smith, R. B., and J. P. Evans (2007), Orographic precipitation and water vapor fractionation over the southern Andes, *J. Hydrometeorol.*, *8*(1), 3–19, doi:10.1175/JHM555.1.

SRH (2012), Sistema Nacional de Información Hídrica, edited by Servicio de Recursos Hídricos, Secretaría de Obras Públicas, Buenos Aires. www.hidricosargentina.gov.ar

Stern, L. A., and P. M. Blisniuk (2002), Stable isotope composition of precipitation across the southern Patagonian Andes, *J. Geophys. Res.*, *107*(D23), 4667, doi:10.1029/2002JD002509.

Stewart, M. (1975), Stable isotope fractionation due to evaporation and isotopic exchange of falling waterdrops: Applications to atmospheric processes and evaporation of lakes, *J. Geophys. Res.*, *80*(9), 1133–1146, doi:10.1029/JC080i009p01133.

Sturm, C., G. Hoffmann, and B. Langmann (2007), Simulation of the stable water isotopes in precipitation over South America: Comparing regional to global circulation models, *J. Climate*, *20*(15), 3730–3750, doi:10.1175/JCLI4194.1.

Vera, C., et al. (2006), The South American low-level jet experiment, *Bull. Am. Meteorol. Soc.*, *87*(1), 63, doi:10.1175/BAMS-87-1-63.

Viale, M., and F. A. Norte (2009), Strong cross-barrier flow under stable conditions producing intense winter orographic precipitation: A case study over the subtropical central Andes, *Weather Forecast.*, *24*(4), 1009, doi:10.1175/2009WAF2222168.1.

Viale, M., and M. Nuñez (2011), Climatology of winter orographic precipitation over the subtropical central Andes and associated synoptic and regional characteristics, *J. Hydrometeorol.*, *12*(4), 481–507, doi:10.1175/2010JHM1284.1.

Vogel, J., W. Lerman, and W. Mook (1975), Natural isotopes in surface and groundwater from Argentina, *Bull. Sci. Hydro.*, *20*(2), 203–221, http://iahs.info/hsj/hsjindex.htm#Top.

Vuille, M., R. S. Bradley, M. Werner, R. Healy, and F. Keimig (2003), Modeling δ18O in precipitation over the tropical Americas: 1. Interannual variability and climatic controls, *J. Geophys. Res. Atmos.*, *108*(D6), 4174, doi:10.1029/2001JD002039.

Wara, M. W., A. C. Ravelo, and M. L. Delaney (2005), Permanent el nino-like conditions during the Pliocene warm period, *Science*, *309*(5735), 758–761.

Wassenaar, L. I., P. Athanasopoulos, and M. J. Hendry (2011), Isotope hydrology of precipitation, surface and ground waters in the Okanagan Valley, British Columbia, Canada, *J. Hydrol.*, *411*(1–2), 37–48, doi:10.1016/j.jhydrol.2011.09.032.

Worden, J., et al. (2007), Importance of rain evaporation and continental convection in the tropical water cycle, *Nature*, *445*(7127), 528–532, doi:10.1038/nature05508.